



LAWRENCE
LIVERMORE
NATIONAL
LABORATORY

Studies of Passive Films on Friction Stir Processed and Laser Peened Ni-Al Bronze

J. Farmer, P. Legrand, T. McNelley, S. Menon, L.
Brewer, L. Hackel

June 8, 2011

Department of Defense Corrosion Conference 2011
Palm Springs, CA, United States
July 31, 2011 through August 5, 2011

Disclaimer

This document was prepared as an account of work sponsored by an agency of the United States government. Neither the United States government nor Lawrence Livermore National Security, LLC, nor any of their employees makes any warranty, expressed or implied, or assumes any legal liability or responsibility for the accuracy, completeness, or usefulness of any information, apparatus, product, or process disclosed, or represents that its use would not infringe privately owned rights. Reference herein to any specific commercial product, process, or service by trade name, trademark, manufacturer, or otherwise does not necessarily constitute or imply its endorsement, recommendation, or favoring by the United States government or Lawrence Livermore National Security, LLC. The views and opinions of authors expressed herein do not necessarily state or reflect those of the United States government or Lawrence Livermore National Security, LLC, and shall not be used for advertising or product endorsement purposes.

Studies of Passive Films on Friction Stir Processed and Laser Peened Ni-Al Bronze

Joseph C. Farmer
Lawrence Livermore National Laboratory
7000 East Avenue
Livermore, CA 94550
United States of America

Peggy S. Legrand
Naval Postgraduate School
1 University Circle
Monterey CA 93943
United States of America

Terry R. McNelley
Naval Postgraduate School
1 University Circle
Monterey CA 93943
United States of America

Sarath K. Menon
Naval Postgraduate School
1 University Circle
Monterey CA 93943
United States of America

Luke N. Brewer
Naval Postgraduate School
1 University Circle
Monterey CA 93943
United States of America

Lloyd A. Hackel
Metal Improvement Company
7655 Longard Road
Livermore CA 94551
United States of America

ABSTRACT

The friction stir processing (FSP) and welding of nickel aluminum bronze (NAB) is used for a variety of naval applications, with the possibility of laser peening (LP) being used as a method for densification and mitigation of residual tensile stress. This paper investigates the beneficial effects of FSP on NAB passivity, and provides important benchmark data for future studies. Further enhancement of FSP NAB through application of LP will be discussed in subsequent papers, using the data presented here as a basis of comparison. This work shows that FSP has a beneficial effect on both the microstructure of this alloy, as well as on the integrity of the passive film formed in chloride electrolytes, including natural seawater. In addition to using a variety of characterization techniques to determine the effects of friction stir processing on microstructure, including scanning electron microscopy (SEM) with focused ion beam milling, we have used cyclic polarization (CP) and electrochemical impedance spectroscopy (EIS) to develop an understanding of passive film behavior for this material in the as-received state, as well as after friction stir processing. A variety of interfacial impedance models have been explored for fitting the data, including transmission line models. Results on this important alloy, before and after processing will be presented.

Key words: nickel aluminum bronze, NAB, friction stir processing, FSP, friction stir welding, FSW, laser peening, LP, cyclic polarization, CP, electrochemical impedance spectroscopy, EIS, scanning electron microscopy, SEM

INTRODUCTION

Friction stir processing (FSP) and friction stir welding (FSW) of nickel-aluminum bronze (NAB) is a promising combination of processing and material for a variety of important naval applications. Such processing has a dramatic effect on both the microstructure of this alloy, as well as on the integrity of the passive film formed in chloride electrolytes, including natural seawater. In addition to using a variety of characterization techniques to determine the effects of FSP on microstructure, including scanning electron microscopy (SEM) with energy dispersive analysis of X-rays (EDAX) and focused ion beam (FIB) milling, we have used in situ electrochemical techniques including cyclic polarization (CP) and electrochemical impedance spectroscopy (EIS) to develop an understanding of passive film behavior for this material in the as-received (AR) and FSP states.

Cyclic polarization of AR and FSP NAB has shown that that FSP decreases the number of electrochemically active sites for oxygen reduction. Electrochemical impedance spectroscopy has enabled the effects of FSP on passive film structure and stability to be understood more fully than otherwise possible. Equivalent circuit models of the AR & FSP NAB interfaces have been developed to fit impedance spectra. Such modeling has shown that passive films formed on multiple phases in the alloy (α, β, κ) require multiple time-constant model to reflect three phases lying beneath the corresponding multi-phase passive film.

Improvements in the passivity of FSP NAB have been demonstrated with EIS of NAB in the AR and FSP conditions. A wide variety of impedance models have been explored for fitting the data, including the well-known Unified Transmission Line (UTL) models. After the investigation of tens-of-models, we have found a relatively simple impedance model that fits the data very well, with parameters reflecting changes in passivity as samples transition from the AR to the FSP state. This electrical circuit model has multiple time constants, which were found essential for adequately fitting the impedance data, and is also conceptually consistent with microstructural observations of the interface.

Nickel Aluminum Bronze (NAB) possesses a unique combination of high strength, high fracture toughness, and high ductility, with casting being used as the main manufacturing process for forming it into shapes of practical importance, such as propellers for ships [1-2]. During casting, the relatively slow cooling rates experienced can lead to large coarse grains. Such coarse microstructure and porosity have been found to cause decreased material performance. Porosity makes the propeller more prone to cavitations, thereby decreasing the service life of the propeller. The use of Friction Stir Processing (FSP) is a state-of-the-art processing technique that can be used both grain refinement and the elimination of porosity and voids in the near-surface region of the material. NAB is a two-phase Cu-based alloy with 5 to 8.5-9.5 wt. % Al, 4.0-5.0 wt. % Ni, 3.5-4.5 wt. % Fe, 0.8-1.5 wt. % Mn, with less than 0.10 wt. % Si and less than 0.03 wt. % Pb. The composition of this alloy has been published in a number of papers, and is repeated in Table 1 [3]. Three metallurgical phases would be expected to appear during cooling, depending upon composition and rate:

1. α -phase: Cu-rich solid-solution (FCC)
2. κ -phase: Al-rich intermetallic (NiAl and Fe_3Al)
3. β -phase: Retained martensitic structure

Friction Stir Welding (FSW) and Friction Stir Processing (FSP) are closely related processes [McNalley et al. 2004]. FSW is a solid-state joining process where a rotating pin traverses a joint between two adjacent pieces of metal, plastically deforming and frictionally heating the two mating surfaces, mixing the material at the interface together, thereby creating a weld. Unlike other joining processes that cause melting, FSW has no fusion zone. FSP is a solid-state grain-refining process wherein a rotating pin is first forced into the work piece, and is then forced to traverse along the surface of work piece. FSW is used to join very large sheets of aluminum to construction of airplanes, and to join air frames to

the overlying airfoil. It has also been investigated as a means of performing underwater repair of ship hulls and other structures. During FSP stirring causes frictional heating, plastic deformation, and grain refinement. Any insight gained into FSP and the impact of this process on passive film stability and corrosion resistance is also therefore relevant to FSW.

EXPERIMENTAL PROCEDURE

The surface of NAB plate were subjected to FSW with a tool rotation speed of 1200 revolutions per minute (rpm) and a travel speed of approximately 2 inches per minute (ipm). Composite of metallurgical cross-sections showing the transverse view of a typical alloy sample subjected to FSP are shown in Figure 1. In this figure, the stir zone (SR), the heat affected zone (HAZ), and the thermomechanically affected zone (TMAZ) are all clearly visible.

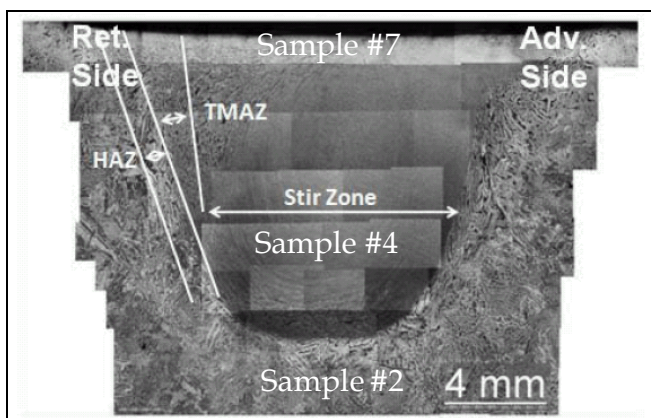


Figure 1: Composite of metallurgical cross-sections showing the transverse view of a typical alloy sample subjected to FSP, with the general location of samples 2, 4 and 7 that will be discussed here identified. The stir zone (SR), the heat affected zone (HAZ) and the thermo-mechanically affected zone (TMAZ) are all clearly shown in this cross section.

The corrosion of NAB has been previously investigated [4]. The enhancement of NAB passivity with FSW has been studied with both cyclic polarization (CP) and electrochemical impedance spectroscopy (EIS), and for the first time reported here. A standardized electrochemical test station used for this study is comprised of: (1) a multichannel potentiostat procured from Gamry Corporation, which are co-located inside the cases of the personal computers used for their control; (2) a three-electrode electrochemical cell constructed from borosilicate glass (Pyrex); a working electrode assembly (with AR or FSP NAB samples); (3) a graphite rod counter electrode; (4) a silver-silver chloride (Ag/AgCl/KCl) reference electrode; (5) electrolyte consisting of aqueous solution of NaCl or natural seawater; and (6) temperature control system capable of heating the electrolyte to temperatures near the boiling point (well above 100°C in the case of some salt solutions), without any evaporative loss of water.

A standard silver silver-chloride electrode, filled with near-saturation potassium chloride solution, is used as the reference, and communicates with the test solution via a Luggin probe placed in close proximity to the working electrode, thereby minimizing Ohmic losses. Numerical corrections for the reference electrode junction potential have been estimated, and have been found to be insignificant. The electrochemical cell is equipped with a water-cooled junction to maintain reference electrode at ambient temperature, thereby maintaining integrity of the potential measurement, and a water-cooled condenser to prevent the loss of volatile species from the electrolyte.

It has been found that Electrochemical Impedance Spectroscopy (EIS) is an effective means of revealing differences in passive film behavior on NAB as a result of FSP. After the investigation of tens-of-models, we have found a relatively simple impedance model that fits the data very well, with parameters reflecting changes in passivity as samples transition from the AR to the FSP state. This

electrical circuit model has multiple time constants, which were found essential for adequately fitting the impedance data, and is also conceptually consistent with microstructural observations of the interface. From FIB SEM results, we know that such a passive film consists of several types of discrete passive film regions, with each type covering specific metallurgical in the underlying polycrystalline alloy. Results on this important alloy, before and after processing will be presented in subsequent sections of this publication. However, principles underlying EIS as it is applied to FSP NAB are first reviewed.

RESULTS

The microstructures FSP NAB surfaces have been investigated with scanning electron microscopy (SEM) with the results shown in Figures 2 through 5. This image shows two distinctive regions: (1) the stir zone; and (2) the eutectoid region. The stir zone consists of finely dispersed regions of α -phase and transformed β -phase. The FCC α -phase region with fine κ_{ii} (Fe_3Al). The eutectoid region consists of α -phase with precipitated κ_{iii} (NiAl) crystallites. The larger precipitates seen in the eutectoid region are κ_{ii} (Fe_3Al), surrounded with κ_{iii} (NiAl) crystallites. These may serve as pit initiation sites.

An SEM image of the surface of an AR NAB sample (identified as Sample #2) after corrosion testing is shown in Figure 2. The morphology of the surface suggests discrete regions covered with different types of oxide: (1) one type of oxide covering the lamellar eutectoid region, which consists primarily of the α - and κ_{iii} -phases; and (2) a second type of oxide covering the FCC α -phase region. The adherent oxide film covering the lamellar eutectoid region shows faceted growth. As shown in Figures 3 and 4, pitting is clearly visible on the oxide covered surface, and appears to be predominantly within the oxide-covered lamellar eutectoid regions. An SEM image of the surface of an FSP NAB sample (identified as Sample #7) after corrosion testing is shown in Figure 5. These corroded FSP stir-zone regions appear to be uniformly oxidized. In this case, the oxide crystals on the sample surface are much finer after FSP (diameter ~ 0.2 mm) than in the AR condition (diameter ~ 1 mm).

The anodic branches of the cyclic polarization (CP) curves shown in Figures 6 and 7 reflect the rate of the oxidation reactions that occur during the anodic portion of the potential scan, and show reproducibility. These oxidation reactions include both anodic dissolution, as well as oxide film growth (passive film formation). In contrast, the cathodic branch shown in this CP curve reflects the rates of the reduction reactions that occur during the cathodic portion of the potential scan. Based upon this CP testing, it is concluded that friction stir processing (FSP) modifies the nickel aluminum bronze (NAB) surface in a way to enhance passive film stability, thereby leading to higher required potentials for passive film breakdown. It is further concluded that FSP lowers the current density associated with the cathodic reduction reactions required to drive corrosion. This observation is consistent with a postulated loss of electro-catalytically active sites on surface for reduction reactions. Active sites could be lost due to crystallites serving as active sites being swept beneath the surface of the alloy during FSP, and the three-dimensional (3D) surface area of these sites reduced by grain refinement induced by FSP. Passive films formed on FSP NAB appear to have: (1) greater passive film stability, even when polarized at very high anodic potential; and (2) suppressed electro-catalytic activity, which lowers the rates of those reduction reactions required to drive anodic oxidation.

Electrochemical impedance spectroscopy (EIS) has been used to investigate the integrity of the passive film formed on AR NAB (Sample #2), and samples with various area fractions modified by FSP (Samples #4 and #7), as shown in Figures 8 and 9. The surfaces of Samples #4 and #7 are completely modified by FSP. Increases in the amplitude of the complex impedance at low frequency (below 1,000 Hz) are correlated with increased modification of the surface by FSP, which appears to cause the formation of a passive film with finer oxide crystallites, thereby increasing the resistance of the passive film, along with the corrosion resistance. This EIS data shows unambiguously that FSP can improve the passivity and corrosion resistance of complex alloys like NAB. A more complete understanding of the

large changes in the EIS data with FSP modification requires the development of mathematical models, which will be discussed in forthcoming sections of the paper.

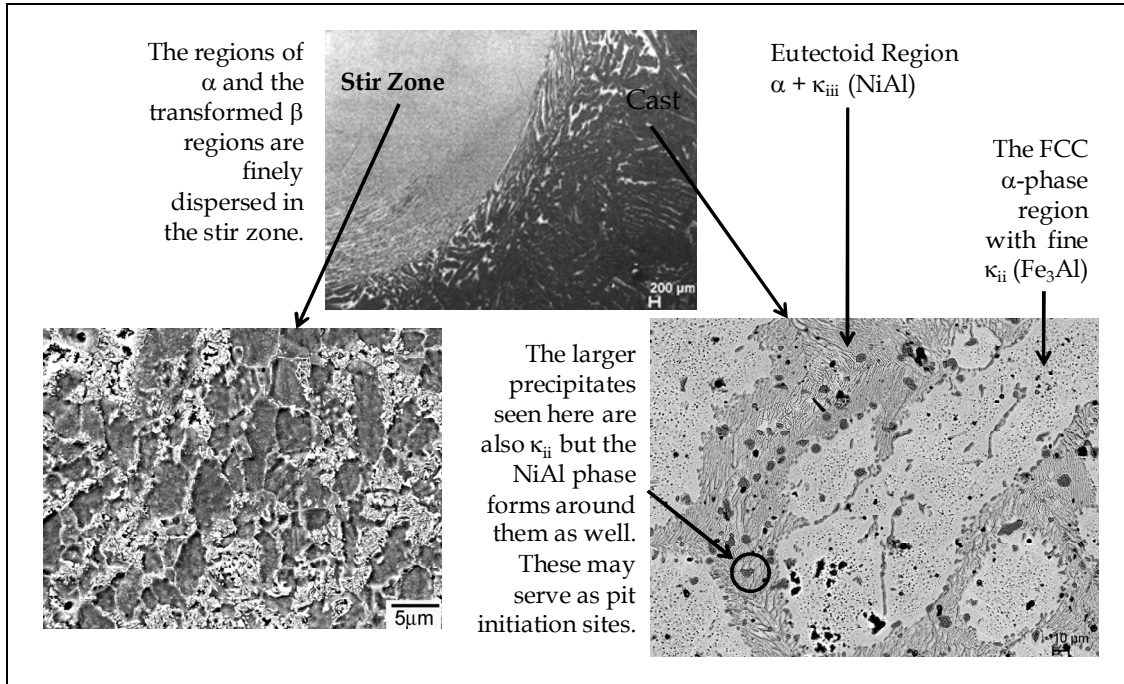


Figure 2: Microstructure of FSP NAB (1200 rpm & 2 ipm)

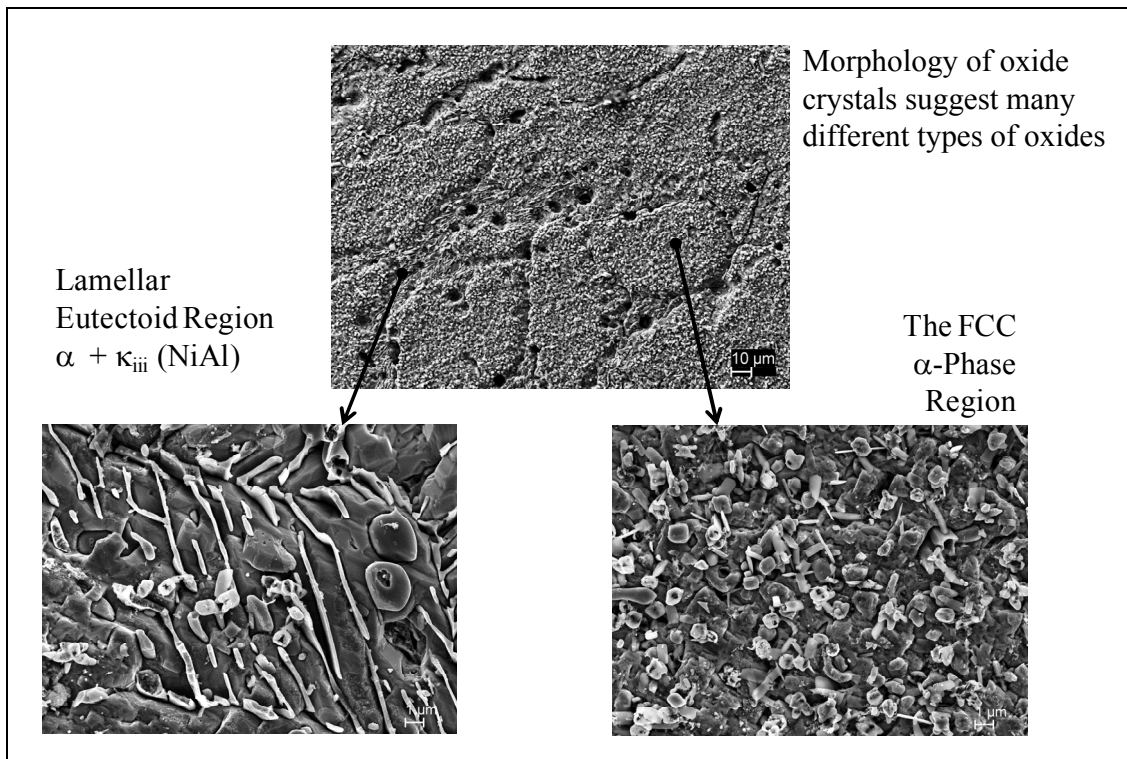
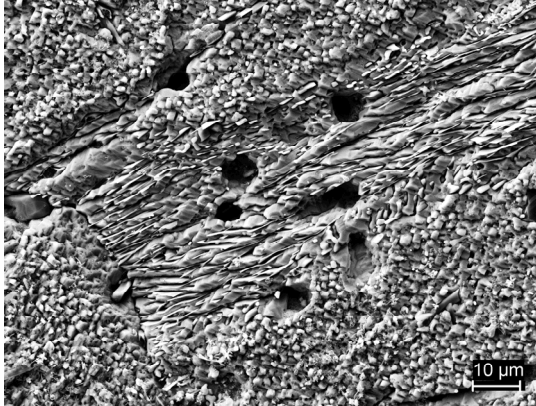


Figure 3: As-Cast NAB (Sample #2) Regions Following Corrosion Testing

As cast regions (Sample #2) after corrosion – these micrographs show at least two different surface regions with pitting clearly visible



The lower figure shows some faceted growth of the adherent oxide followed by the more porous oxide crystals on the surface

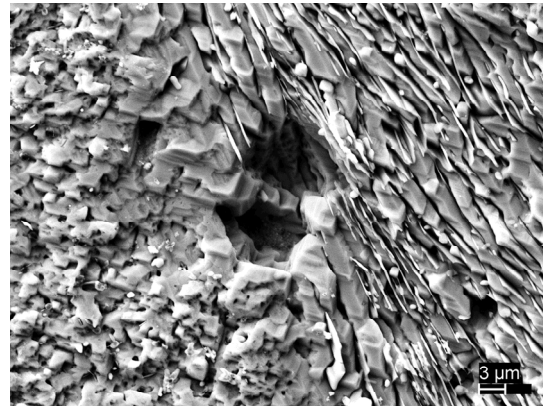
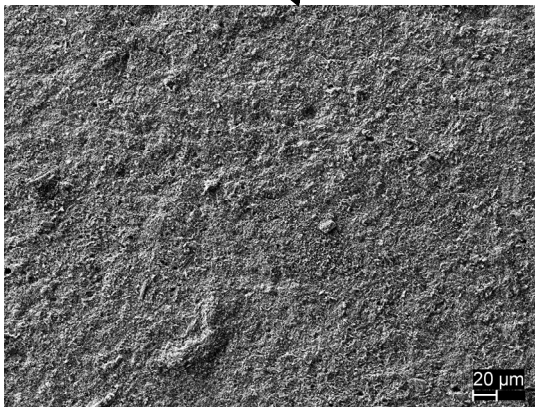


Figure 4: As-Cast NAB (Sample #2) Regions Following Corrosion Testing

FSP stir-zone regions (Sample #7) after corrosion – the surface appears to be uniformly oxidized



Oxide crystals on the sample surface are much finer after FSP ($\sim 0.2 \mu\text{m}$ verses $\sim 1 \mu\text{m}$ on as cast) ... the fine lamellar regions are probably also oxidized as seen here

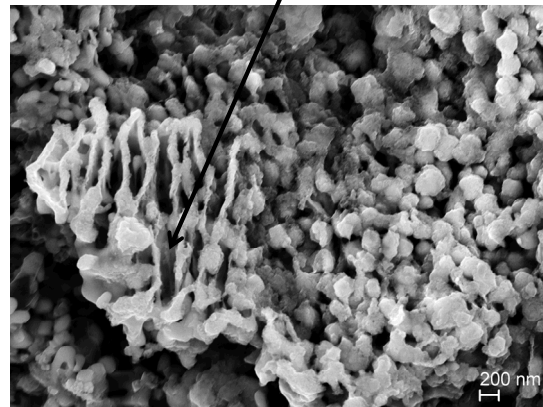


Figure 5: As-Cast NAB (Sample #7) Regions After Corrosion Testing

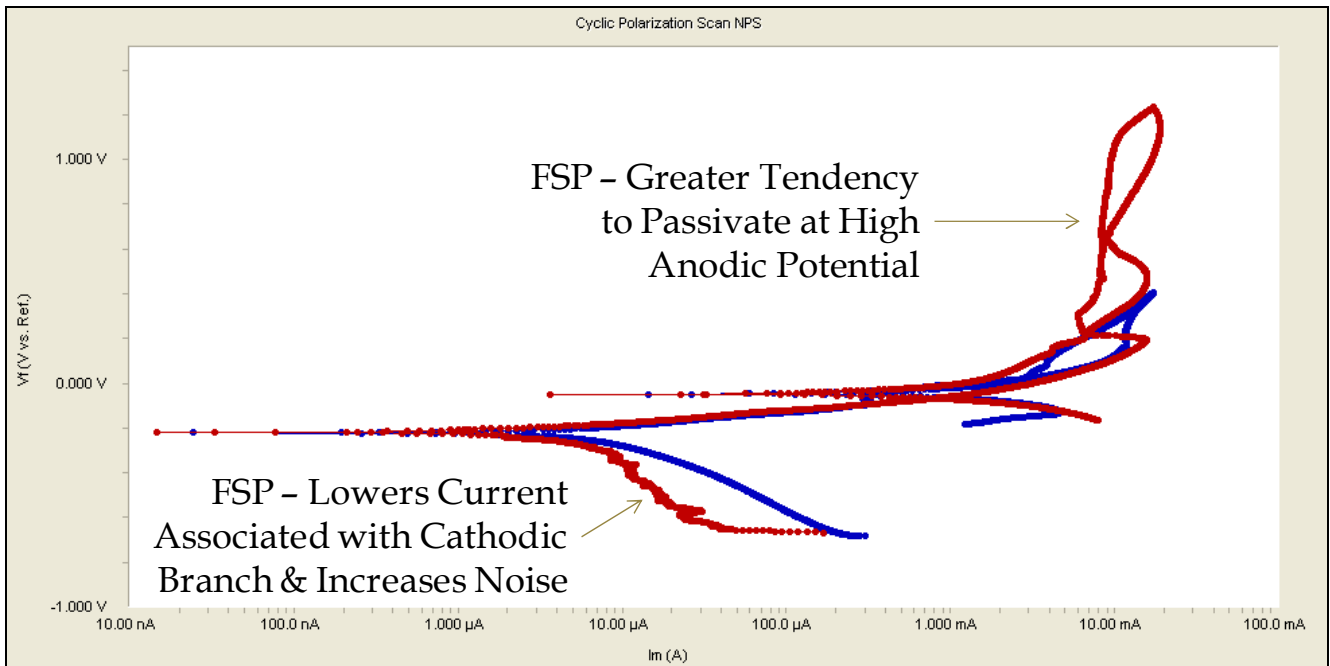


Figure 6: Cyclic Polarization (CP) of Friction Stir Processed Nickel Aluminum Bronze (FSP NAB) in Seawater at 30°C: 1 = Below Surface with No FSP; 7 = Outer Surface with FSP

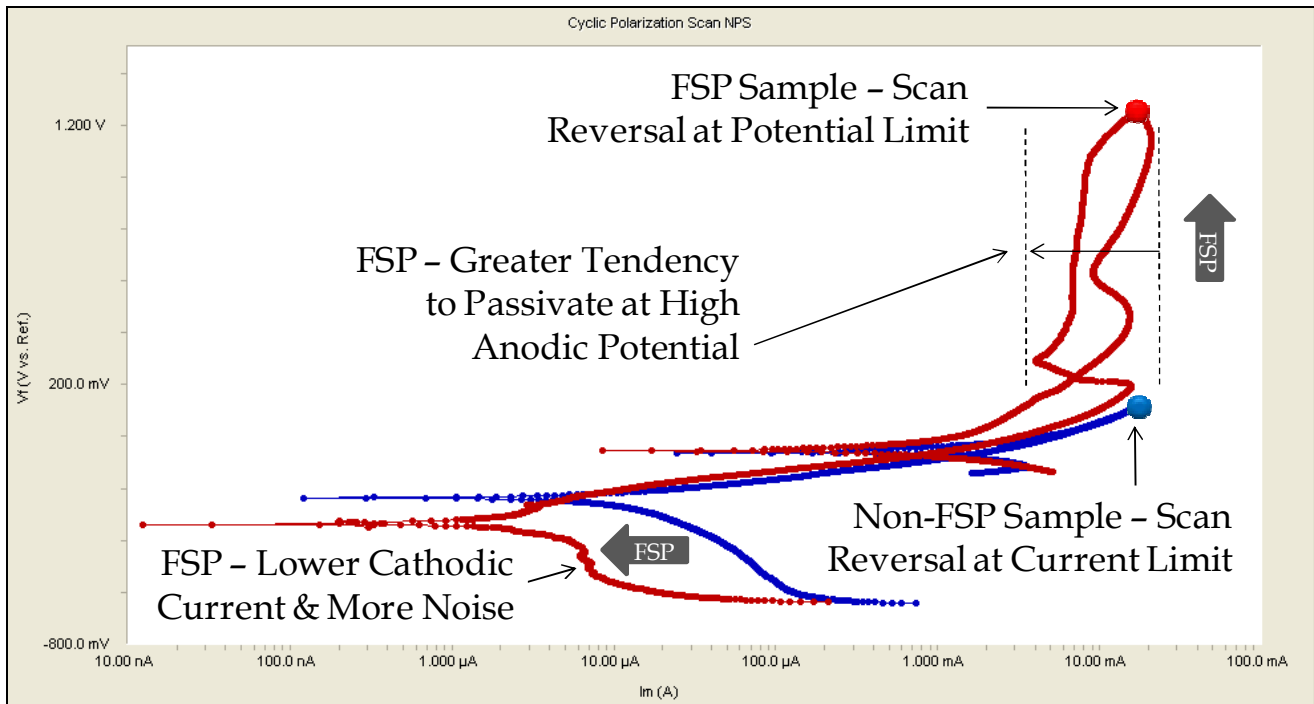


Figure 7: Cyclic Polarization (CP) of Friction Stir Processed Nickel Aluminum Bronze (FSP NAB) in Seawater at 30°C: 1 = Below Surface with No FSP; 7 = Outer Surface with FSP

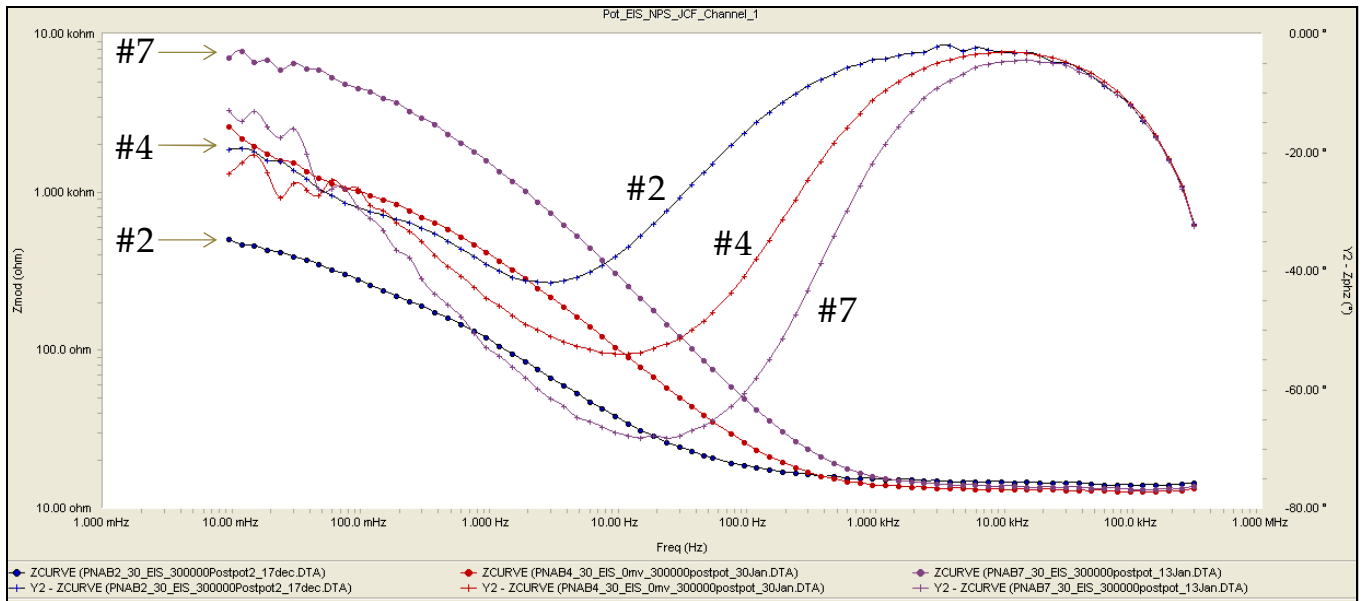


Figure 8: Effect of FSP Surface Modification on NAB Passivity in Seawater at 30°C. The amplitude of the complex impedance is plotted against the left axis (10 to 10,000 ohms), the phase angle ϕ plotted against the right axis (0 to -80 degrees), and the frequency range extends from 0.010 to 300,000 Hertz.

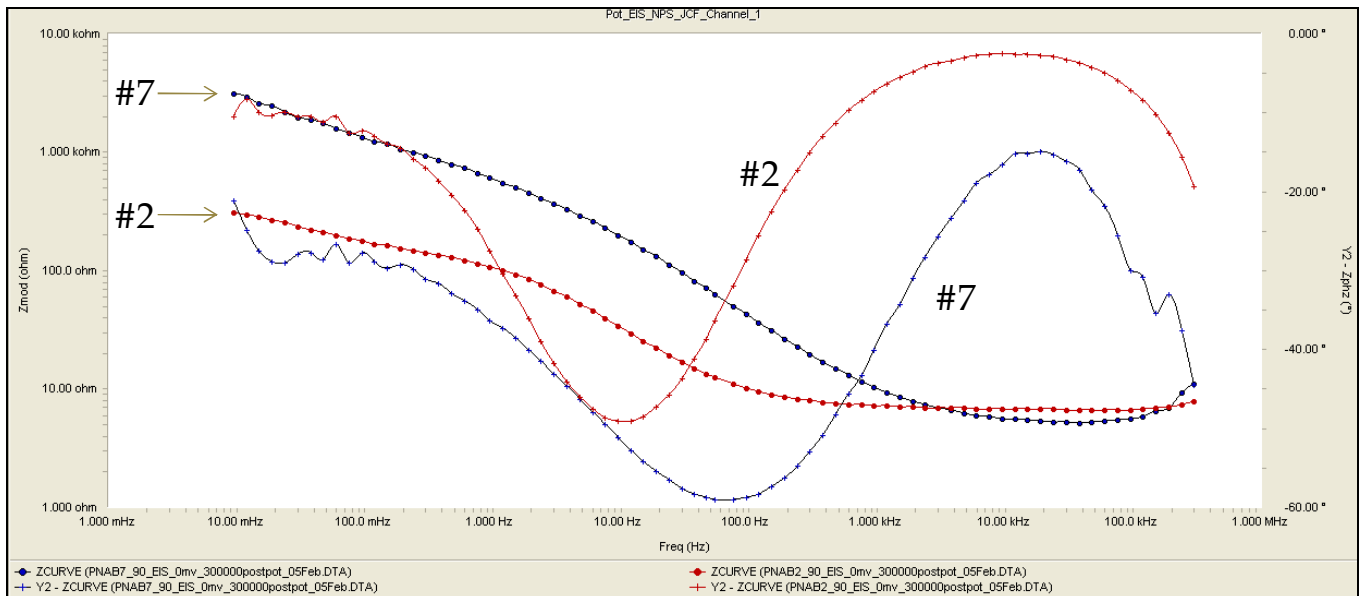


Figure 9: Effects of FSP Surface Modification on NAB Passivity in Seawater at 90°C. Axes are identical to those shown in the previous figure.

After the investigation of several models with a wide range of complexity, we have found that a relatively simple impedance model that is conceptually consistent with SEM observations of the interface is capable of fitting the EIS data very well, with parameters reflecting changes in passivity as samples transition from the AR to the FSP state. From our SEM observations, we now know that such the passive film formed on AR NAB consists of at least two distinct types, with each type covering a specific metallurgical phase in the underlying polycrystalline alloy. The morphology of the surface suggests discrete regions covered with different types of oxide: (1) one type of oxide covering the lamellar eutectoid region, which consists primarily of the α - and κ_{ii} -phases; and (2) a second type of oxide covering the FCC α -phase region. Development of the model begins with an expression for the overall complex admittance the exposed surface:

$$\hat{Y}_{total} = x_{\alpha} \hat{Y}_{\alpha} + x_{\beta} \hat{Y}_{\beta} + x_{\kappa_{ii}} \hat{Y}_{\kappa_{ii}} + x_{\kappa_{iii}} \hat{Y}_{\kappa_{iii}} + x_{\kappa_{iv}} \hat{Y}_{\kappa_{iv}} + x_z \hat{Y}_z \quad \text{(Equation 1)}$$

Each term in this expression for the admittance corresponds to the passive film covering the metallurgical phase indicated by the subscript (Figure 11). The last term is included to account for unknown phases, or perhaps the effect of pitting on the interfacial impedance.

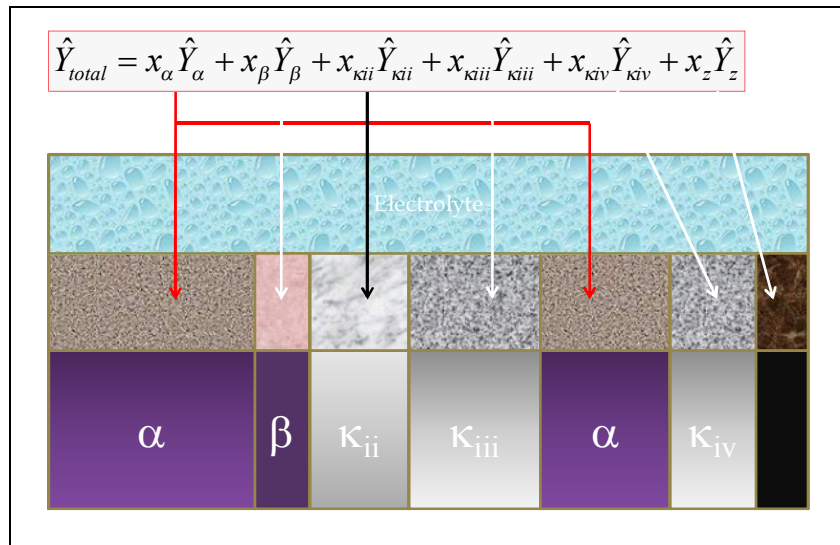


Figure 10 – FSP NAB EIS Model #0 Simple Single Time Constant RC Network

Given the complexity of the AR FSP surface evident in the SEM images, it is not surprising that the simple single time-constant model was found to be incapable of fitting the data. The impedance models explored to explain the EIS data for AR and FSP NAB include: Model #1, a series combination of Warburg, Gerischer and Unified Transmission Line (UTL) impedances (Figure 12); and Model #6, a series combination of Warburg, Gerischer and three parallel RC-circuit impedances (Figure 13). It was found that more complicated multiple time-constant models (Models #1 and #6) were required to fit the data over the entire range of frequency extending from 0.01 Hz to 300 kHz. Fitting was done with a simplex-type optimization program that determined model parameters by seeking out the minimum in the sum-of-squares surface (minimum in error between prediction and observation). Supporting discussions of EIS and its application can be found in the published literature [5-7].

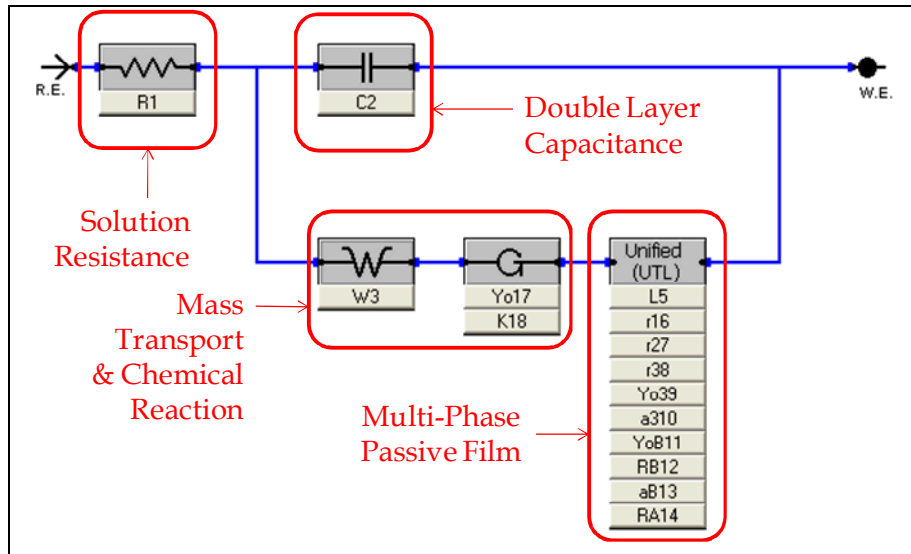


Figure 11: FSP NAB EIS Model #1 – A Series Combination of Warburg, Gerischer, and Transmission Line Impedances

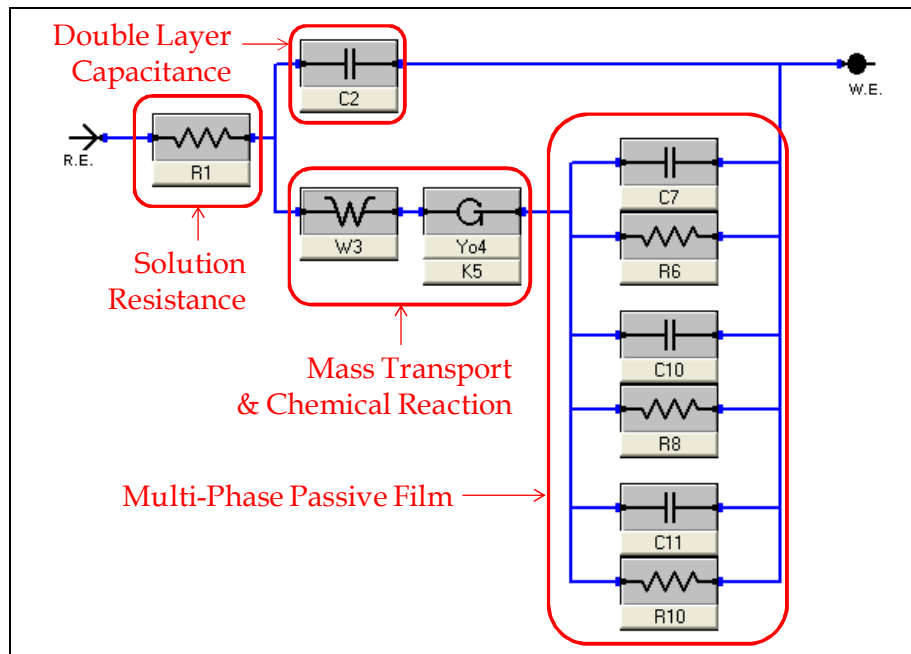


Figure 12: FSP NAB EIS Model #6: A Series Combination of Warburg, Gerischer, and Three Parallel RC-Circuit Impedances

Model #1 is a series-parallel combination including a solution resistance, a double layer capacitance, the Warburg impedance, the Gerischer impedance, and a unified transmission line (UTL) impedance is capable of fitting the data for both AR and FSP NAB interfaces very well. Model #6 has fewer model parameters than Model 1, and is also capable of fitting these data. This simplified model is a series-parallel combination including a solution resistance, a double layer capacitance, the Warburg impedance, the Gerischer impedance, and three “resistor-capacitor branches” in parallel. Conceptually, both models seem consistent with features seen in the SEM images of the passive film structure. The goodness of fit for Models #1 and Models #6 are evident in Figures 13 and 16. The trends in the parameters for Models #1 and #6 are shown in Figures 17 and 18. In regard to the trend in the parameters for Model #1, the solution resistance and double layer capacitance (R1 and C2) are

independent of FSP, as expected. However, the interfacial resistance values associated with passivity (RB12 and RA14) increase three orders-of-magnitude (1×10^3) moving from the as-received condition (Sample #2 – AR) to the friction stir processed condition (Sample #7 – FSP). The conclusion is that the beneficial effect of FSP on passivity of NAB is clearly evident in the quantitative parameters for the mechanistically based EIS model. While not as dramatic as the changes in the resistance values for Model #1, significant increases in the interfacial resistance parameters (R6 and R8) for Model #6 are also evident. Of the models considered thus far, the conceptual porous film model represented by Model #1 with the UTL impedance element may provide the best representation of the FSP-modified passive film on NAB.

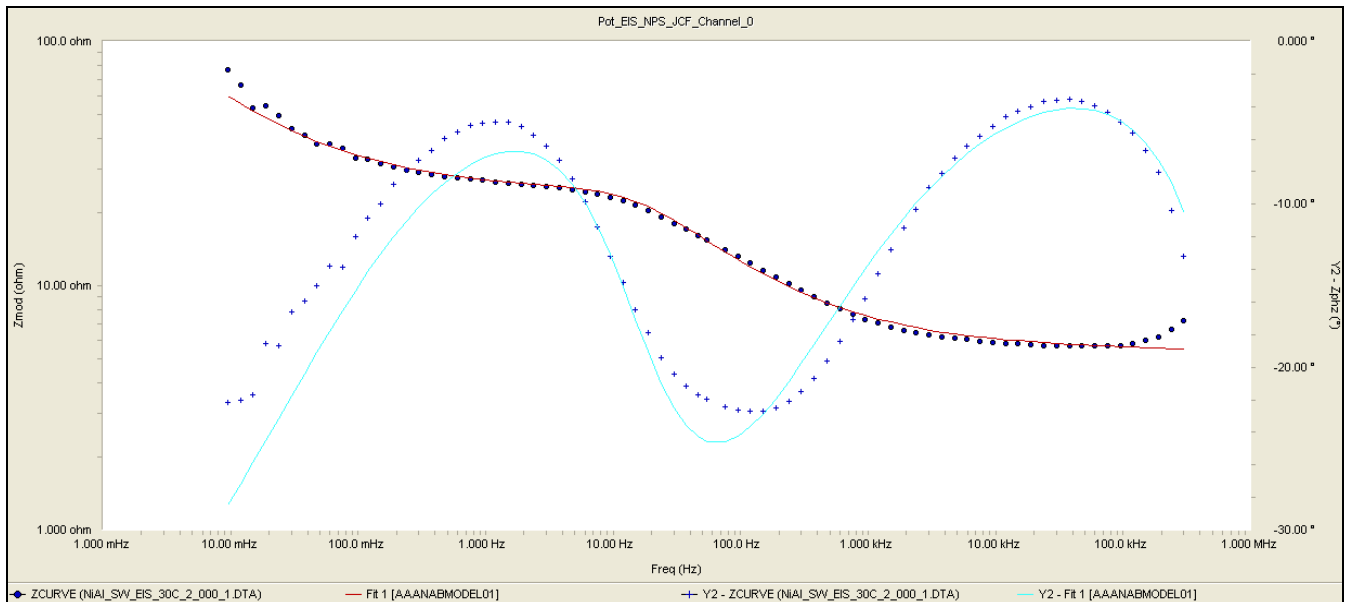


Figure 13 : AR (Sample #2) NAB SW 30°C Data Fit to EIS Model #1: A Series Combination of Warburg, Gerischer and Unified Transmission Line (UTL) Impedances.

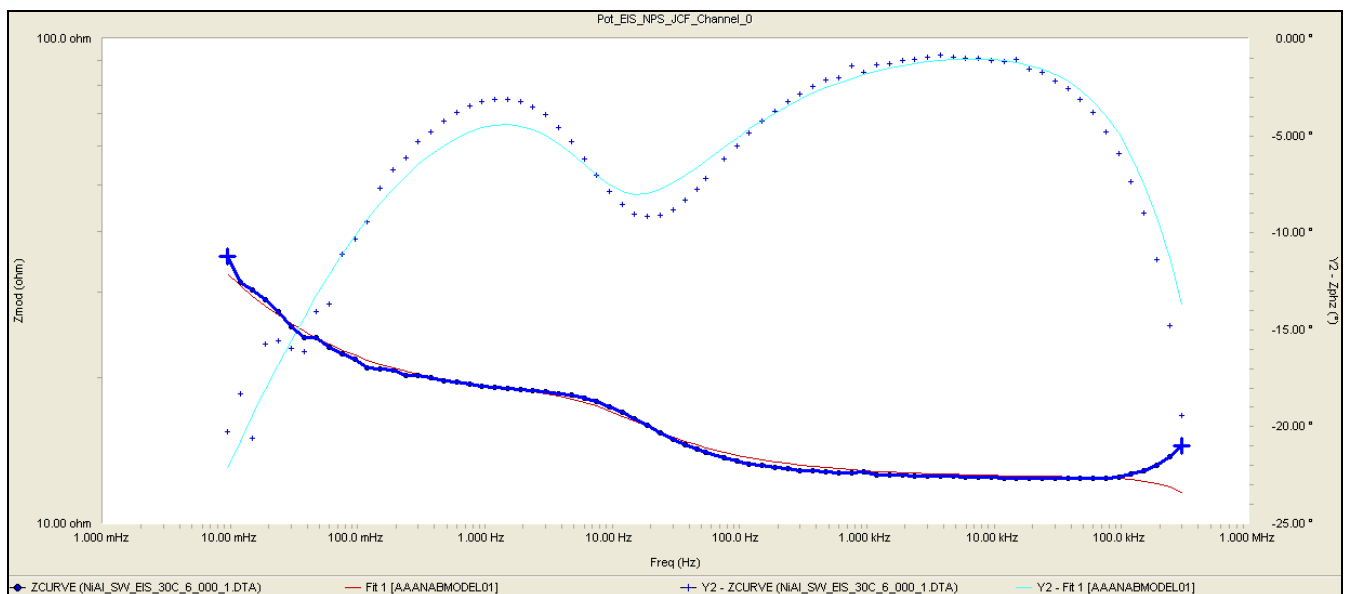


Figure 14: FSP (Sample #6) NAB SW 30°C Data Fit to EIS Model #1: A Series Combination of Warburg, Gerischer and Unified Transmission Line (UTL) Impedances

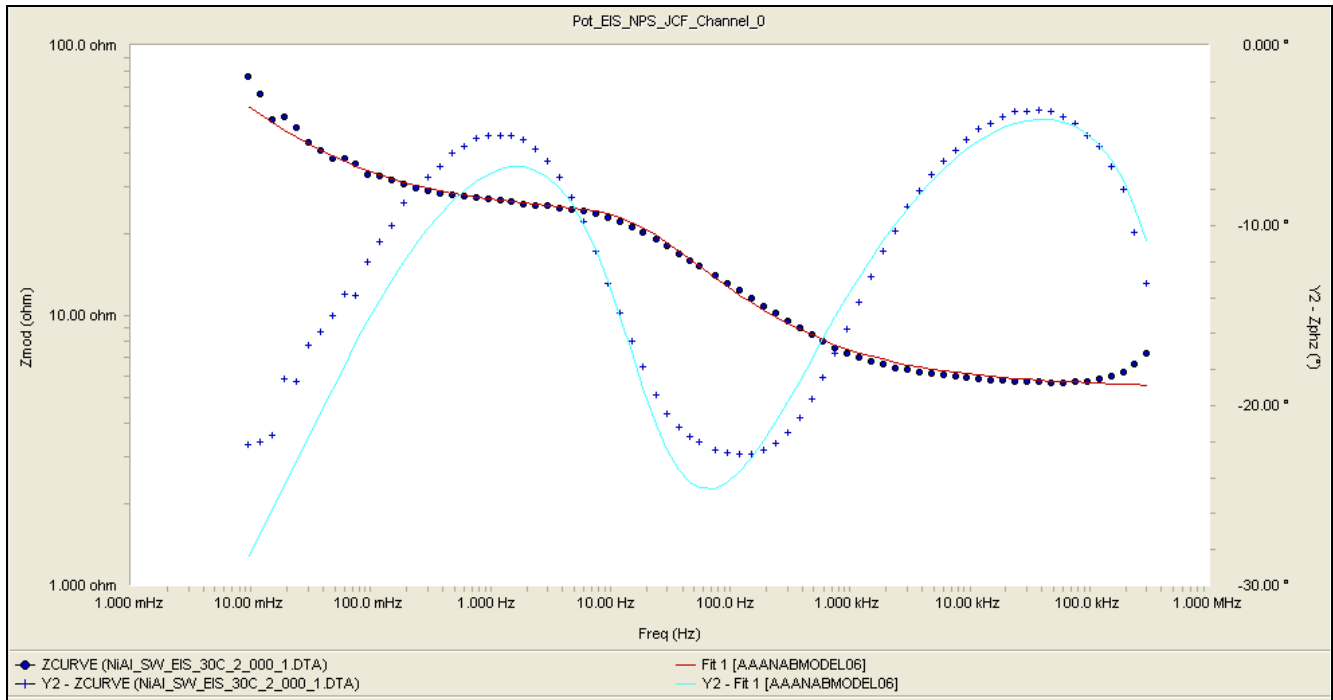


Figure 15: AR (Sample #2) NAB SW 30°C EIS Model #6: A Series Combination of Warburg, Gerischer and Three Parallel RC-Circuit Impedances with Locked Electrolyte Parameters

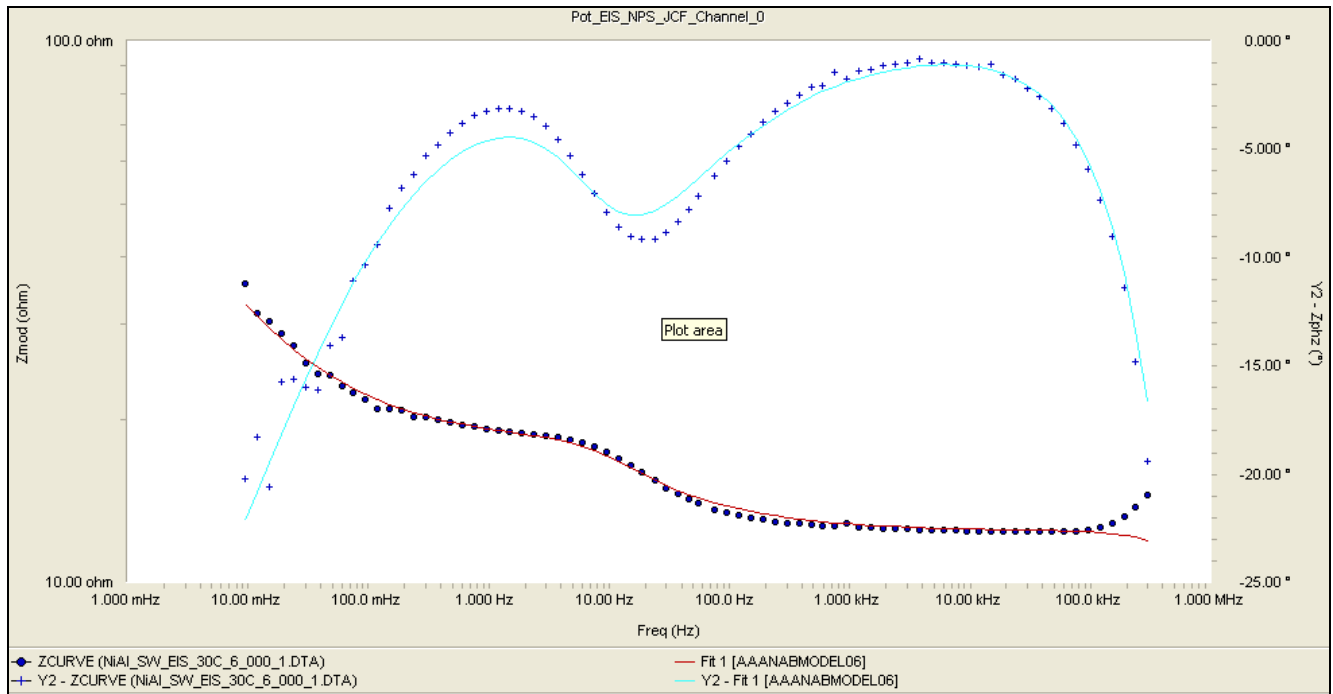


Figure 16: FSP (Sample #6) NAB SW 30°C EIS Model # 6: A Series Combination of Warburg, Gerischer and Three Parallel RC-Circuit Impedances with Locked Electrolyte Parameters

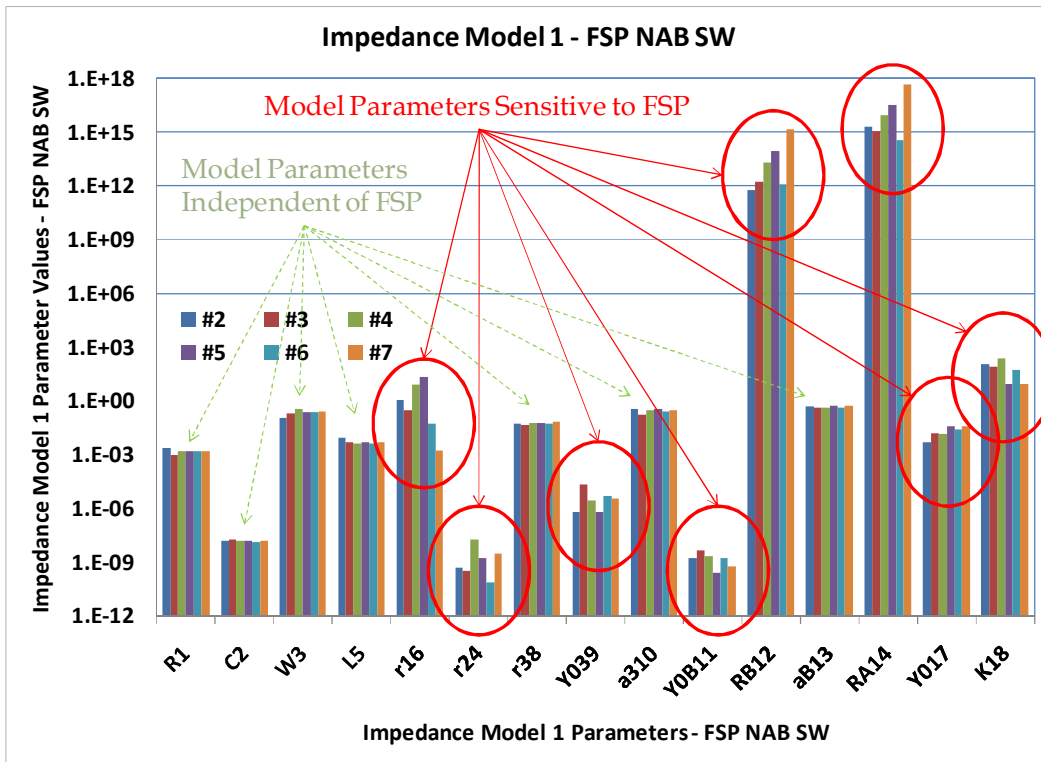


Figure 17 – AR & FSP NAB SW 30°C Data Fit to EIS Model # 1: A Series Combination of Warburg, Gerischer, and Transmission Line Impedances.

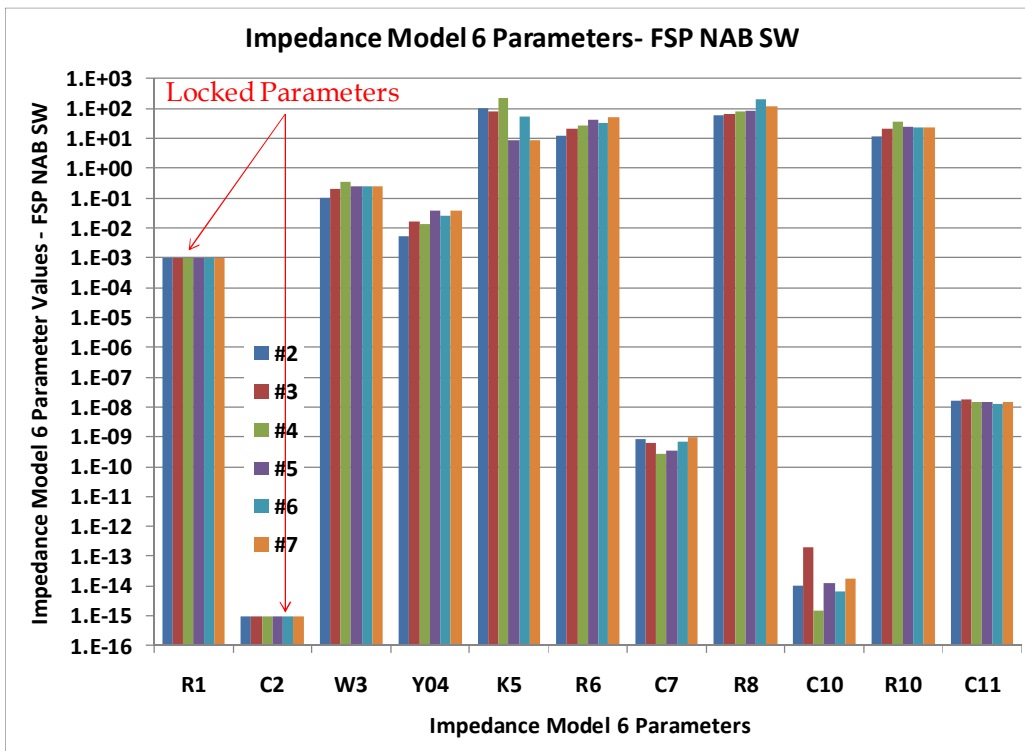


Figure 18: AR & FSP NAB SW 30°C Data Fit to EIS Model # 6: A Series Combination of Warburg, Gerischer, and Three Parallel RC-Circuit Impedances.

CONCLUSIONS

Friction stir processing (FSP) and friction stir welding (FSW) of nickel-aluminum bronze (NAB) is a promising combination of processing and material for a variety of important naval applications. Such processing has a dramatic effect on both the microstructure of this alloy, as well as on the integrity of the passive film formed in chloride electrolytes, including natural seawater. In addition to using a variety of characterization techniques to determine the effects of FSP on microstructure, including scanning electron microscopy (SEM) with energy dispersive analysis of X-rays (EDAX) and focused ion beam (FIB) milling, we have used in situ electrochemical techniques including cyclic polarization (CP) and electrochemical impedance spectroscopy (EIS) to develop an understanding of passive film behavior for this material in the as-received (AR) and FSP states.

SEM of AR and FSP NAB samples, before and after corrosion testing, has revealed dramatic changes in the morphology of the passive film as a result of this type of surface modification. The morphology of the surface suggests discrete regions covered with different types of oxide: (1) one type of oxide covering the lamellar eutectoid region, which consists primarily of the α - and κ_{III} -phases; and (2) a second type of oxide covering the FCC α -phase region. The adherent oxide film covering the lamellar eutectoid region shows faceted growth. Pitting is clearly visible on the oxide covered surface, predominantly on the oxide-covered lamellar eutectoid region. Corroded FSP stir-zone regions appear to be uniformly oxidized, with oxide crystals on the surface modified with FSP much finer (diameter ~ 0.2 μm) than in the as-received condition (diameter ~ 1 μm).

Cyclic polarization of AR and FSP NAB has shown that that FSP decreases the number of electrochemically active sites for oxygen reduction. Electrochemical impedance spectroscopy has enabled the effects of FSP on passive film structure and stability to be understood more fully than otherwise possible. Equivalent circuit models of the AR & FSP NAB interfaces have been developed to fit impedance spectra. Such modeling has shown that passive films formed on multiple phases in the alloy (α , β , κ) require multiple time-constant model to reflect three phases lying beneath the corresponding multi-phase passive film.

The significant effects of FSP on passive film behavior are being studied with Electrochemical Impedance Spectroscopy (EIS). Electrochemical impedance spectroscopy (EIS) has been used to investigate the integrity of the passive film formed on AR NAB, and samples with various area fractions modified by FSP. Increases in the amplitude of the complex impedance at low frequency (below 1,000 Hz) are correlated with increased modification of the surface by FSP, which appears to cause the formation of a passive film with finer oxide crystallites, thereby increasing the resistance of the passive film, along with the corrosion resistance. This EIS data shows unambiguously that FSP can improve the passivity and corrosion resistance of complex alloys like NAB.

ACKNOWLEDGEMENTS

Lawrence Livermore National Laboratory (LLNL) is operated by Lawrence Livermore National Security, LLC, for the U.S. Department of Energy, National Nuclear Security Administration under Contract DE-AC52-07NA27344. The enabling support of LLNL is greatly appreciated. Karl van Bibber, Vice President of Research, Knox Millsaps, Professor and Chairman of Mechanical and Aerospace Engineering, and Terry McNelley, Distinguished Professor of Mechanical and Aerospace Engineering, are gratefully acknowledged for their role making this collaborative work possible.

This document was prepared as an account of work sponsored by an agency of the United States government. Neither the United States government, nor Lawrence Livermore National Security LLC, nor any of their employees make any warranty, expressed or implied, or assumes any legal liability or responsibility for the accuracy, completeness, or usefulness of any information, apparatus, product, or

process disclosed, or represents that its use would not infringe privately owned rights. Reference herein to any specific commercial product, process, or service by trade name, trademark, manufacturer, or otherwise does not necessarily constitute or imply its endorsement, recommendation, or favoring by the United States government or Lawrence Livermore National Security, LLC. The views and opinions of authors expressed herein do not necessarily state or reflect those of the United States government or Lawrence Livermore National Security, LLC, and shall not be used for advertising or product endorsement purposes.

REFERENCES

1. T.R. McNelley and K. Oh-Ishi. "Microstructural Modification of As-Cast NiAl Bronze by Friction Stir Processing," *Metallurgical and Materials Transactions A*, 35A (2004) pp. 2004-2951.
2. T.R. McNelley and K. Oh-Ishi, "The Influence of Friction Stir Processing Parameters on Microstructure of As-Cast NiAl Bronze," *Metallurgical and Materials Transactions A*, 36A, (2005) pp. 1575-1585.
3. F. Hasan, A. Jahanafrooz, G.W. Lorimer, N. Ridley, "The Morphology, Crystallography, and Chemistry of Phases in As-Cast Nickel-Aluminum Bronze," *Metallurgical and Materials Transactions A*, 13, 8 (1982) pp. 1337, 1982.
4. . M. Pidaparti, B.S. Aghazadeh, A. Whitfield, A.S. Rao, G.P. Mercer, "Classification of Corrosion Defects in NiAl Bronze Through Image Analysis," *Corrosion Science* (Accepted July 7, 2010) [www.elsevier.com/locate/corsci, doi:10.1016/j.corsci.2010.07.017].
5. A.J. Bard, L.R. Faulkner, *Electrochemical Methods, Fundamentals and Applications* (John Wiley & Sons, New York, NY, 1980).
6. H. Shih, *Electrochemical Impedance Spectroscopy (EIS), Technology and Applications* (The Electrochemical Society, Pennington, NJ, 2006).
7. M.E. Orazem, *General Electrochemistry and Introduction to Impedance Spectroscopy, Motivation, Representation of Impedance Date, Impedance Measurement, and Discussion* (The Electrochemical Society, Pennington, NJ, 2005).
8. J.C. Farmer, S. Menon, P. Legrand, "Effect of FSP on the Electrochemical Activity and Passive Film Stability of Ni-Al Bronze" (Extended Abstracts, 219th Meeting of the Electrochemical Society Meeting, Montreal, Canada, May 2011).